Caballero-Mancebo, E.; Moreno Rodríguez, JM.; Corma Canós, A.; Díaz Morales, UM.; Cohen, B.; Douhal, A. (2018). How does the Surface of Al-ITQ-HB 2D-MOF Condition the Intermolecular Interactions of an Adsorbed Organic Molecule?. ACS Applied Materials & Interfaces. 10(23):20159-20169. https://doi.org/10.1021/acsami.8b04222

How does the Surface of Al-ITQ-HB 2D-MOF Condition the Intermolecular Interactions of an Adsorbed Organic Molecule?

Elena Caballero-Mancebo[a], José María Moreno[b], Avelino Corma[b], Urbano Díaz[b], Boiko Cohen[a*] and Abderrazzak Douhal[a*]

[a]Departamento de Química Física, Facultad de Ciencias Ambientales y Bioquímica, and INAMOL, Universidad de Castilla-La Mancha, Avenida Carlos III, S/N, 45071 Toledo, Spain.

[b]Instituto de Tecnología Química, Universitat Politecnica de Valéncia-Consejo Superior de Investigaciones Científicas (UPV-CSIC), Av. de los Naranjos s/n, 46022 Valencia, Spain.

*corresponding author: Boyko.Koen@uclm.es; Abderrazzak.Douhal@uclm.es

ABSTRACT

In this work, we unravel how the 2D-Al-ITQ-HB metal organic framework changes the interactions of Nile Red (NR) adsorbed on its surface. Time-resolved emission experiments indicate the occurrence of energy transfer between adsorbed NR molecules, in abnormally long time constant of 2-2.5 ns, getting shorter (~0.25 ns) when the concentration of the surface adsorbed NR increases. We identify the emission from local excited state of aggregates, and charge-transfer and energy transfer between adsorbed molecules. Femtosecond emission studies reveal an ultrafast process (~425 fs) in the NR@Al-ITQ-HB composites, assigned to an intramolecular charge transfer in NR molecules. Comparison of the observed photobehavior with those of NR/SiO_2 and NR/Al_2O_3 composites suggests that the occurrence of energy transfer in the NR@MOF complexes is a result of specific and non-specific interactions, reflecting the different surface properties of Al-ITQ-HB that are of relevance to the reported high catalytic activity. Our results provide new knowledge for further researches on other composites aiming toward a better understanding of photocatalytic and photonic processes within MOFs.

KEYWORDS: hybrid materials, composites, defects, energy and charge transfer, ultrafast spectroscopy, Nile Red, aggregates, silica and alumina particles.

1. INTRODUCTION

Metal-organic frameworks (MOFs), a class of hybrid materials made from organic linkers and inorganic nodes, have emerged as novel porous materials that are gaining relevance in different scientific fields due to their wide range of applications. [1-14] For example, in photonics, MOFs have been used as energy donors and as acceptors in different photonic antennas.[15] The donor or the acceptor entity can be adsorbed on the surface or encapsulated by the nanomaterial, where the energy transfer (ET) efficiency will depend on the distance between the partners and their orientations, in addition to possible electronic changes due to specific and non-specific interactions with the supporting/encapsulating host.[16-19] Al-ITQ-HB, a recently synthesized mesoscopic framework with layer-based structure acting as a support for molecular systems, may facilitate the occurrence of the ET process between chromophores interacting with its surface (Scheme 1A).[20] The two dimensional (2D) structure of Al-ITQ-HB is formed by 4-heptylbenzoic acid (HB) as the organic spacer and octahedral aluminum clusters as metal nodes.[20] This unique laminal framework, with very rich external surface and internal space, is expected to affect the distribution and reaction of organic molecules interacting with it. Therefore, it is of great relevance to (photo)catalysis and photonics to elucidate the interaction of organics with this MOF.

One can use well-known dyes/molecular probes to understand the influence of the surface properties of this kind of material on the formed composites. Organic molecules that undergo intramolecular charge transfer (ICT) and therefore large change in their electronic configuration are used as probes of local environment properties. Nile Red (NR) is a well-known dye, sensitive to the nature of its environment.[21-23] Its photobehavior, both in solution and in restrictive chemical and biological environments, has been studied theoretically and experimentally.[21, 24, 25] It undergoes an ICT[25, 26] in its

first singlet excited-state (S_1), due to the presence in its structure of both an amino and keto groups, which have electron donating and withdrawing character, respectively.[25, 26] It has been widely used as a molecular probe to study the properties of different materials, including MOFs, by encapsulating it within their porous structure.[22, 27-32] The behaviour of NR encapsulated within the Al-ITQ-HB hybrid has been recently reported.[33] Under specific experimental conditions of making the composites, we have shown that the trapped NR molecules form several populations (as aggregates and monomers), interacting in two different regions of the MOF structure characterized with different polarities. However, how the surface properties of this MOF affect the photophysical behaviour of the adsorbed NR to different extent remains unexplored. By changing the procedure of making the NR@Al-ITQ-HB composites we managed to predominantly favor the adsorption of NR molecules on the Al-ITQ-HB surface.

Herein, we show how the Al-ITQ-HB surface affects the photobehavior of the adsorbed NR molecules (Scheme 1B). Steady-state UV-visible experiments show the presence of several adsorbed NR species, revealing a broad absorption band and a narrow emission spectrum, indicating a fast non-radiative deactivation of some excited and adsorbed molecules. The absorption and emission spectral overlap suggests the possibility of ET process. Time-resolved emission experiments on different composites, where we changed the amount of the adsorbed dye on the MOF surface, show a photoevent having a time constant of 2-2.5 ns, assigned to ET between adsorbed NR species. This event becomes faster (~0.25 ns) when the concentration of adsorbed NR increases. We compare the results with those using NR powder and NR/SiO_2 and NR/Al_2O_3 composites, showing remarkable difference in the properties of the Al-ITQ-HB surface and its influence on the photochemistry of the adsorbed molecular probe. Femtosecond (fs) emission experiments reveal two ultrafast components, assigned to an

ICT process (~ 425 fs), and vibrational cooling (~9 ps) of the excited adsorbed NR. The results provide better understanding of the surface properties of Al-ITQ-HB, promoting its use as a supporting material for photochemical reactions and photophysical processes, which may give raise to potential applications in (photo)catalysis and photonics.

2. EXPERIMENTAL METHODS

2.1 Materials and Synthesis of the NR@M-ITQ MOFs

Al-ITQ-HB MOF was prepared according to the procedures reported in the literature.[20] Briefly, it was synthesized from equimolar quantities of $AlCl_3.6H_2O$ (3.1 mmol) and 4-heptylbenzoic acid (3.1 mmol), which were dissolved in two different solutions with 15 mL DMF each. The two solutions were mixed and the resulting slurry was introduced into a stainless steel autoclave, and heated at 150ºC for 24 hours under autogenous pressure and static conditions. Once cooled to room temperature, the solution was filtered with distilled water. The sample was activated in methanol for 24 hours in order to efficiently remove the remaining unreacted linker and solvent molecules. Finally, the material was isolated and dried under vacuum at room temperature.

For the spectroscopic studies, Nile Red (NR, Sigma-Aldrich, purity >98.0%) was adsorbed on the surface of the material using the following procedure. Firstly, a solution of NR with a known concentration ($1x10^{-3}$M, $1x10^{-4}$M and $1x10^{-5}$M) in dichloromethane (DCM) was prepared. Then, 50 mg of the MOFs were added to 1 mL of the NR/DCM solution, and the mixture was stirred for 24 h at room temperature. Finally, in contrast with the previous work,[33] where the formed composites were washed several times in order to remove the excess of NR and resulting in blue colored samples (NR@Al-ITQ-HB (I) in Scheme 1B), the solvent was eliminated by evaporation in this case, making NR being mainly deposited on the surface of the MOF, and giving purple colored

composites (NR@Al-ITQ-HB (II) in Scheme 1B). For the synthesis of NR/SiO_2 and NR/Al_2O_3 composites, using SiO_2 (Sigma-Aldrich, particle size <50 nm) and Al_2O_3 (Sigma-Aldrich, particle size <50 nm) nanoparticles (NPs), we followed the same procedure as for the MOF composites, by adding 50 mg of the NPs to 1 mL of the dye solution. The mixture was stirred and the solvent was evaporated.

2.2 Structural, Spectroscopic and Dynamic Measurements

The XRD analysis of the materials was carried out with a Philips X'PERT diffractometer equipped with a proportional detector and a secondary graphite monochromator. Data were collected stepwise over the $2^o \leq 2\theta \leq 20^o$ angular region, with steps of 0.02^o 2θ, 20s/step accumulation time and CuKα (λ=1.54178 Å) radiation. XRD patterns (Figure S1) showed the mesoscopic organization achieved for Al-ITQ-HB material when 4-heptylbenzoic acid was used as organic spacer, where one intense (100) diffraction signal was recorded at low 2θ angles range at ~35 Å, being associated with mesoporous materials with long-range hexagonal order. The XRD pattern of NR@Al-ITQ-HB sample shows that the morphology of the hybrid MOF-type materials was maintained after the incorporation of NR molecules. The morphology of the Al-ITQ-HB material was corroborated also by transmission electronic microscope (TEM, JEOL JEM2100F electron microscope operating at 200 keV), where the mesoscopic character of the hybrid material was observed, although it was difficult to detect the free mesoporous cavities due to the low homogeneity of the crystals (Figure S2). Most of the particles has an average size of 100 – 200 nm. The samples were prepared directly by dispersing the powders onto carbon copper grids.

The steady-state UV-visible absorption and fluorescence spectral measurements were carried out using JASCO V-670 and FluoroMax-4 (Jobin-Yvone)

spectrophotometers, respectively. The diffuse reflectance spectra were measured using a 60-mm integrating sphere (ISN-723) and corrected with the Kubelka Munk function. The picosecond time-resolved emission experiments have been recorded employing a time-correlated single-photon counting (TSCPC) system previously described.[34] The samples were excited by either 40 ps-pulsed (~1 mW, 40 MHz repetition rate) diode-lasers (PicoQuant) centered at 470 nm and 635 nm, or by a femtosecond optical parametric oscillator (Inspire Auto 100) pumped by 820-nm pulses (90 fs, 2.5 W, 80 MHz) from a Ti:sapphire oscillator (MaiTai HP, Spectra Physics) to generate the excitation beam at 550 nm (~15-20 mW). The instrument response function (IRF) is ~70 and ~35 ps for the diode laser and optical parametric oscillator, respectively. The fluorescence signal was gated at a magic angle (54.71), and monitored at a 90° angle to the excitation beam at discrete emission wavelengths. The decays were deconvoluted and fitted to a multiexponential function using the FLUOFIT package (PicoQuant) allowing single and global fits. The quality of the fits as well as the number of exponentials were carefully selected based on the reduced χ^2 values (which were always below 1.2) and the distributions of the residuals. The femtosecond time-resolved emission decays were collected in solid state using a fluorescence up-conversion technique in reflection mode.[33] The system consists of a Ti:sapphire oscillator (MaiTai HP, Spectra Physics) to generate the excitation beam at 470 nm (~15-20 mW). The polarization of the laser was set to the magic angle with respect to the fundamental beam (940 nm). The solid sample was placed in a 1-mm-thick randomly moved cell. The fluorescence emission was collected at 0° with respect to the pump laser. It was focused and gated with the fundamental femtosecond beam to obtain the sum frequency (SFG) signal. The IRF of the apparatus (measured as the reflected signal of the pump signal) was ~300 fs (full width at half-maximum, FWHM) at the excitation wavelength. To analyze the decays, a multi-

exponential function convoluted with the IRF was used to fit the experimental data. In all cases, the errors for the calculated time components were smaller than 15%. All the experiments were performed at room temperature (295 K).

3. RESULTS AND DISCUSSION

3.1 Steady-State of NR@Al-ITQ-HB with Different Initial Dye Concentrations

To begin with, we studied the steady-state behaviour of NR interacting with Al-ITQ-HB surfaces. Figure 1 shows the normalized UV-visible absorption and emission spectra of three NR@Al-ITQ-HB samples made with different initial dye concentrations ($[NR]_0$, $1x10^{-5}$, $1x10^{-4}$ and $1x10^{-3}$M). Figure S3 exhibits the unnormalized spectra of these composites. We believe that the contribution of NR molecules located within the framework channels is not significant compared to that of NR on the surface. Scheme 1B shows the difference in colors of both composites made using different synthesis procedures. The distinction of the colors suggests different types of interactions between the adsorbed NR molecules from one side and with the MOF framework on the other one. These interactions depend on the synthesis procedure and the location of the NR molecules. The UV-visible absorption spectrum of the composites prepared with $[NR]_0$ of $1x10^{-5}$M shows a broad (full width at half maximum of intensity, FWHM ~5890 cm^{-1}) and structureless band with the maximum of absorbance at 576 nm and a blue edge shoulder at ~450 nm. The main band is broad and deviates from a Gaussian shape, which suggests the presence of several absorbing species.

The emission spectrum consists of a single structureless band with its intensity maximum at 640 nm (Figure 1). The spectral position and shape show no dependence on the excitation wavelength (Figure S4A). The band is narrower (FWHM ~2130 cm^{-1}) in comparison with the absorption one (~5890 cm^{-1}), indicating that some of the excited

surface-adsorbed species relax to the ground state through efficient non-radiative pathways. The absorption and emission spectra show strong overlap, which will facilitate the interaction between the adsorbed NR species. These interactions may result in a homo-transfer of energy between the dye molecules (Figure S4A).[16]

To further characterize the photochemistry of NR adsorbed on the surface of Al-ITQ-HB, we have studied their photobehavior at two additional $[NR]_0$. The sample with $[NR]_0$ $1x10^{-4}$ M shows an absorption spectrum with a broad band (FWHM ~6300 cm^{-1}) with maximum of absorption at 552 nm (Figure 1). The broadness of the band also suggests a higher heterogeneity of the absorbing species. The emission band has its intensity maximum at 659 nm, which results in a Stokes shift of 2950 cm^{-1} (Figure 1). This shift is larger than the one observed in the less concentrated composite (~1800 cm^{-1}), indicating that the initial NR concentration used to prepare the composites affects their photobehavior. The emission spectrum shows no significant variation with the excitation wavelength (Figure S4B). While the absorption spectrum reveals a relatively broader band in comparison with the less concentrated sample (~6300 cm^{-1} vs ~5900 cm^{-1}), the emission band is narrower (~1340 cm^{-1} vs ~2130 cm^{-1}). This result suggests that even though there is a higher heterogeneity in the distribution of NR populations at the surface of Al-ITQ-HB, giving different absorbing species, the excited structures mainly relax following a narrow deactivation pathway or the emission quantum yields of these emitters are very different, and weak for some of them.

The composite prepared using a higher $[NR]_0$ ($1x10^{-3}$ M) shows a behaviour similar to the previous one. The maximum of the broad absorption spectrum is at 558 nm, and of its emission spectrum at 670 nm (Figure 1). In this case, the fluorescence spectrum exhibits a small shift to longer wavelengths as the excitation wavelength increases (Figure S4C) suggesting that the red-emitters absorb at longer wavelengths. Figure S5 shows that

the absorption and emission spectral overlap is larger for the composites having the lowest used $[NR]_0$, which is normally reflected in higher probability of energy transfer between NR adsorbed molecules.[18, 19] However, using a higher $[NR]_0$ to make the composites a larger red shift and narrower emission bands are recorded, which indicates the presence of additional processes that affect the overall photobehavior. The excitation spectra of NR@Al-ITQ-HB surfaces are shown in Figure S6. The spectra present maxima of intensities similar to the absorption ones, with the only notable change observed at the high-energy side of the main band (< 500 nm). This reflects the opening of fast non-radiative channels upon excitation to higher energies of S_1. Note that the absorption is not high in this region.

3.2 Picosecond Behavior of Adsorbed NR

3.2.1 Interrogating Different Adsorbed NR Species on Al-ITQ-HB Surface

In order to understand the behaviour of excited NR adsorbed on Al-ITQ-HB surfaces, we carried out time-resolved emission experiments with picosecond resolution (time-correlated single-photon counting, TCSPC, time resolution ~20 ps). Figure 2 shows the emission decays of the composites, using three different $[NR]_0$ (10^{-5}, 10^{-4} and 10^{-3}M) to make the composites. The presentations are in linear and logarithmic scales, collected at different observation wavelengths and excited at 470 nm. Tables 1, 2 and 3 give the obtained parameters: the time constants (τ_i) and the pre-exponential factors (a_i) normalized to 100 from multiexponential global fits of the decays. The photodynamics of the less concentrated sample (10^{-5}M) reveals a triexponential behaviour, with time components of 0.46, 2.50 and 4.77 ns. Note that the NR@Al-ITQ-HB composites prepared in a different way where NR is predominantly encapsulated do not show such long rise time in the emission decays.[33] The contribution of the longest component increases with the observation wavelength, and becomes the only decaying component

from 650 nm. The intermediate (2.5 ns) one appears as a decay at the blue side of the emission spectra and as a rise from 675 nm.

The contribution of the shortest component (0.45 ns), which is present only at the higher energy side of the emission spectra (550 – 625 nm), decreases until 650 nm and disappears at longer wavelengths. Thus, we assign it to the emission of surface-adsorbed NR population that relaxes from locally excited (LE) states. Similar values (0.3 – 0.7 ns) have been recorded in the whole emission spectra of NR encapsulated within MOF structures and were assigned to LE states and H-aggregates.[33] These results suggest that the value of the time constant associated with the relaxation from the LE state of NR to the ground state is unaffected independent on the location of the dye (on the surface or within its framework). We assign the 2.5-ns component to an ET process between adsorbed NR molecules on the surface of Al-ITQ-HB. Finally, the ~4.8 ns component is ascribed to the emission lifetimes of the photoproduced NR species as a result of the ET process. It should be noted that the lifetime for the photoproduced charge transfer (CT) state as a result of the ICT in NR has a comparable value (3-5 ns) to the emission lifetimes shown in this work.[33] Thus, we cannot exclude contribution of this species to the emission decays. Furthermore, we did not observe any evidence for the presence of ET process in the composites when NR was predominantly encapsulated within the MOF structure. Note also that the ICT in NR occurs in hundreds of femtosecond, a time shorter than the time-resolution of the employed TCSPC set up (~ 20 ps). Below we will examine this event using fs-resolution.

To gain further knowledge of the photodynamics of the composites, we studied the effect of the excitation wavelength on the emission decays. Figure S8A shows a comparison of the results, gating at representative wavelengths upon excitation at 470, 550 and 635 nm (Scheme 2). These excitations allow interrogation of the dynamics of the

different absorbing species adsorbed on the MOF surface, as is suggested by the broad absorption spectrum (Figure 1). Table 1 gives the obtained parameters after multiexponential global fits of the decays compared to the results of 470 nm excitation. Pumping at 550 nm, we observe a small decrease in the shortest (τ_1) and longest (τ_3) time constants. However, the intermediate component (τ_2) shows a more significant decrease in its value, changing from 2.50 to 2.06 ns. The origin of the components is similar to those upon 470 nm excitation. The change in the time constant (τ_2) of ET reflects the excitation of different adsorbed energy donor and acceptor one for which the spectral overlap, the distance and the dipole angles are probably different from those excited at 470 nm.

The decays were also collected upon excitation at 635 nm (lower excess energy at S_1). In this case, we only needed a biexponential fit, giving times of 2.71 and 4.68 ns (Table 1). Both components decay along the whole observation range. Interestingly, we observed no rising component, suggesting absence of ET in these excited NR molecules. While the time constant, 2.71 ns, is comparable to the one associated with the ET process (2-2.5 ns) upon excitation at shorter wavelengths, its behaviour when changing the wavelength of observation (only decay and no rise through the observation spectral range) suggests that it is associated with different species not undergoing energy transfer. We assign this component to the emission decay of a population of stabilized NR aggregates absorbing in the reddest part of the absorption spectrum. The longest time (4.68 ns) has a similar value to the ones obtained when exciting at 470 and 550 nm. The energy of 635 nm excitation is not large enough to access the population of adsorbed NR molecules that act as energy donor. As a result, only the emission lifetime (4.68 ns) of 635-nm excited species is observed (Scheme 2).

3.2.2 Effect of NR Amount on Al-ITQ-HB Surface

To explore the effect of NR initial concentration, we performed ps-experiments on samples having different dye amounts. Figures 2B and 2B' show representative emission decays using $[NR]_0$ $1x10^{-4}$M to get NR@Al-ITQ-HB. Table 2 shows the results using multiexponential global fits of the decays upon excitation at different wavelengths. When the composites are excited at 470 nm, the emission decays exhibit a triexponential behaviour with lifetimes of 0.32, 2.95 and 4.90 ns. The shortest and the intermediate components behave as decay at the bluest and rise at the reddest sides. However, the longest component is present as a decay through the whole spectrum, and its contribution increases with the observation wavelength. We assign the two rising components to ET in the excited NR populations, while the 4.9 ns one to the emission lifetime of the photoproduced NR population following the energy transfer process. The values and the behaviour of the intermediate (~3 ns) and long (~5 ns) time components are comparable to those observed for the composites prepared with $[NR]_0$ 10^{-5}M, and therefore have the same origin. We assign the 0.32-ns component to ET between closely adsorbed NR molecules. At higher concentrations, the distance between NR molecules becomes shorter allowing strong dipole-dipole interaction, and therefore faster energy transfer.[35-37]

This is further confirmed by studying composites of higher $[NR]_0$ ($1x10^{-3}$M, Figure 1 and Table 3). Upon excitation at 470 nm, a triexponential behaviour was needed to get an accurate fit, with lifetimes of 0.22, 1.33 and 3.61 ns. The lifetimes of the intermediate and long components become shorter upon increasing the dye content. This is explained in terms of homoquenching of the NR emission, due to the adsorbed molecules forming aggregates, as it has been reported for other dyes interacting with silica based materials.[38] We also studied the two highest concentration composites upon excitation at different wavelengths (Tables 2 and 3). For the composites made from $[NR]_0$

of $1x10^{-4}$ M, the photobehavior exciting at 550 and 635 nm is comparable to the one observed for the less concentrated sample. For $[NR]_0$ of $1x10^{-3}$M, we found three components. At 550 nm of excitation, we observed a shortening in the time constants, probably due to a higher contribution of the aggregate emissions. Exciting at 635 nm the shortest component (~ 0.15 ns) is observed only as a decay contrary to the behaviour upon excitation at 470 and 550 nm. The excitation at longer wavelengths pumps different populations of adsorbed NR, and at this high concentration, the lifetimes probably correspond to different aggregate populations.

The fluorescence behaviour of the three composites were further studied by recording their Time-Resolved Emission Spectra (TRES). Figures 3 and S7 (Supporting Information) show normalized and non-normalized TRES, respectively, upon excitation at different wavelengths, from the least concentrated (A) to the most (C) concentrated one. Comparing the TRES of the three composites upon excitation at 470 nm, we observe a short lived emission at shorter wavelengths (550 – 650 nm region), and a longer one at 650 – 750 nm. At longer gating time (5 ns), the shape and position of the TRES change and are very similar to those recorded in steady-state conditions (Figure 1 and Figure S10), showing that these longer-time emitters have the highest fluorescence quantum yield and explain why the steady-state emission spectra (Figure 1) are so narrow. These observations are in agreement with the decays shown in Figure 2. Exciting at 550 nm gives a result similar to that upon excitation at 470 nm, confirming the data and previous discussion on the emission decays. The TRES upon excitation at 635 nm do not show any rising component, which may connect two emitters. This is in agreement with the behaviour reflected in Figure S8 and the related previous discussion exciting at the reddest part of the absorption spectrum.

To further comment on the results shown in this part, Table S1 shows the values of the spectral overlap calculated as an absolute area between the absorption and emission spectra of the three different $[NR]_0$ composites, along with the corresponding time constants of the ET processes. The largest overlap is observed for the most diluted complexes, which normally should be reflected in a higher energy transfer probability (shorter time constant). However, we observed the reverse trend. The most concentrated samples display comparable spectral overlap and for both the ET time is about 10 times shorter than in the less concentrated one. We conclude that the shorter distances between the dye molecules produced when the NR concentration on the Al-ITQ-HB surface is higher favor the dipole-dipole interactions, and generate appropriate molecular distributions for more efficient energy transfer (Scheme 2).

3.2.3 NR in Solid State and Supported on Different Nanoparticles

To further explore if the ET process between adsorbed NR molecules is or is not conditioned by the Al-ITQ-HB framework surface, we studied solid NR (powder pellet) as well as NR adsorbed on two types of nanoparticle (NP) surfaces. We have chosen the SiO_2 (< 50 nm) particles to allow study of the photoinduced processes in NR in the absence of metal clusters, and Al_2O_3 (< 50 nm) particles, to simulate the aluminium oxide chemical environment created in the Al-ITQ-HB structure due to the presence of octahedral aluminium nodes in the latest. Although, the MOF and Al_2O_3/ SiO_2 NPs have different size, we believe that the change in the photobehavior of adsorbed NR resides in the specific and non-specific interactions with their surfaces. Scheme 1B shows pictures of NR powder, NR/SiO_2 and NR/Al_2O_3 composites. While solid NR has a brown color, that of the composites is not different from the NR@Al-ITQ-HB studied here. A priori, the adsorbed NR molecules on these 3 materials present the same intermolecular and surface

interactions at the ground state. The absorption and emission spectra, along with the ps-time resolved observations provide more precise information.

Figure S11 shows the UV-visible absorption and emission spectra of NR in solid state. The recorded broad absorption band (~5000 cm^{-1}) with maximum of intensity at 575 nm, and the narrow emission spectrum (1674 cm^{-1}, $\lambda_{max} \approx 640$ nm) are comparable to those of the NR@Al-ITQ-HB composites. Interestingly, the ps-TCSPC experiments on NR powder upon excitation at 470 nm show emission decays very different from those of NR@MOF (Figure 4A). Table S2 gives the obtained values from the multiexponential fit of the emission decays. We used a triexponential function giving times of 67 ps, 0.26 and 1.05 ns. These components decay at all the observation wavelengths, and their contributions are almost constant (~80, ~18 and ~2 %, respectively). These times are significantly shorter than those observed for the NR@Al-ITQ-HB hybrids. Thus, we suggest that these components correspond to different NR aggregates in the solid state due to a strong intermolecular packing. Clearly, the ET process observed in the NR species interacting with Al-ITQ-HB is not observed in the powder of NR. A reason for its absence is probably the strong affinity of NR to form aggregates, which in turn results in a strong coupling between the closely packed molecules and results in ultrafast deactivation.

We have made and studied three NR/SiO_2 NP composites having the same $[NR]_0$ used for the preparation of the MOF hybrid complexes (Figure S12). Figure S13 shows the normalized absorption and emission spectra. The three samples show a broad absorption band (FWHM ~ 4655 cm^{-1}) with a maximum at ~560 nm. The emission bands are narrower than the ones observed for NR@Al-ITQ-HB composites, having FWHM ~1600, 1720 and 2120 cm^{-1}, from the most diluted to the most concentrated samples; while the band maximum shifts to longer wavelengths (from 650 to 670 nm) as the $[NR]_0$

in the composite increases. The observed trends suggest the presence of NR species with strong aggregate character. Figure S14 shows the emission decays of the three composites, and Table S3 gives the obtained parameters from accurate multiexponential global fits. For the most diluted sample, we got time constants of 0.32, 1.85 and 3.75 ns. The shortest component has its highest contribution at bluest wavelengths and disappears from 650 nm. The contribution of the intermediate component (1.85 ns) slightly increases as the observation wavelength gets longer. Finally, we observed the same trend in the contribution of the longest lifetime (3.75 ns).

As the concentration increases, the value of the shortest component slightly decreases from 0.32 to 0.22 ns, the one for the intermediate from 1.85 to 0.57 ns, and the longest one from 3.75 to 1.60 ns. These changes are larger than the errors in the time constant values. The shortest times become shorter upon increasing the content of adsorbed NR on the silica particles, evidencing more efficient aggregates formation. It has been reported that when NR is distributed within heterogeneous porous materials, its molecules adopt different orientations, favoring formation of different types of aggregates.[31-33, 39] Finally, the longest component, observed in the two less concentrated samples (3.75 and 3.21 ns), is assigned to the emission lifetime of monomer species, in similarity with the values observed when NR interacts with other materials.[33, 39] The absence of a rise time (within our ~20 ps resolution) in the signal of NR/SiO_2 NPs indicates that either ET does not occur or it is too fast to be observed with our ps-setup.

NR was also studied when interacting with Al_2O_3 NPs. Three different composites with $[NR]_0$ of $1x10^{-3}$, $1x10^{-4}$ and $1x10^{-5}$M were prepared. Figure S15 and S14 show the recorded UV-visible absorption and emission spectra. The absorption bands are very broad having FWHM of ~5620, 5010 and 4590 cm^{-1}, and maxima at 581, 571 and 567 nm, respectively. The emission spectra consist of narrow bands (FWHM of 2120, 1820

and 1820 cm^{-1}) and intensity maxima located at 660, 646 and 640 nm. The steady-state behaviour is not very different from that of the NR/SiO_2 composites (with comparable shift to longer wavelengths as the NR content gets higher). Figure S17 shows the emission decays of the three composites made with different $[NR]_0$. Table S4 gives the parameters after multiexponential global fits. The most concentrated sample shows a triexponential behaviour with time constant values of 0.17, 0.72 and 1.59 ns, while the intermediate one displays components of 0.18, 0.95 and 2.78 ns, and the less concentrated one gives 0.21, 1.46 and 3.05 ns. This photobehavior is comparable to the one observed for the NR/SiO_2 composites. Therefore, we explain the observed behaviour as a result of formation of different NR aggregates with strong interaction between their molecules. The longest lifetimes in the less concentrated samples corresponds to the emission of adsorbed monomer species.

Figures 4B, 4C and 4D show a comparison of the emission decays gated at 750 nm of NR interacting with the surface of Al-ITQ-HB, SiO_2 and Al_2O_3 NPs with three different $[NR]_0$, respectively. Clearly, when $[NR]_0$ is $1x10^{-3}$M, the decays of NR@Al-ITQ-HB are very different (rise and decay) from those using silica and aluminium particles. When the $[NR]_0$ is $1x10^{-4}$M, the difference is still observable, while the decays become not very different when $[NR]_0$ is lower (10^{-5}M). For this concentration, the emission decays of NR/SiO_2 and NR/Al_2O_3 are longer due to the presence of monomer species, but no rising signal is recorded; while for the NR@Al-ITQ-HB composites using the same $[NR]_0$, we observed a long rising component assigned to ET. Thus, we conclude that the ET between the NR molecules is significantly conditioned and induced by the MOF surface. This constitutes an important finding which is of relevance to the catalytic activity of this MOF. We suggest that defects present on the Al-ITQ-HB surface, probably due to vacancies located on the octahedral aluminium nodes, produce specific interactions

that shape the dye photobehavior. These conditions favor the occurrence of ET between adsorbed NR molecules. High yield has been reported for different organic reactions catalyzed by Al-ITQ-HB.[20] The observed effect of the MOF surface on the photobehavior of NR might be relevant to understand the high catalytic potential of this MOF, and opens the way for a new chemical engineering effort to modify its surface aiming to produce more efficient materials.

3.3 Femtosecond Time-Resolved Fluorescence Study of NR@Al-ITQ-HB

Finally, in order to elucidate the photobehavior of the NR@Al-ITQ-HB composite, at very short time scale, time-resolved experiments with femtosecond (fs) resolution (IRF ~300 fs) were carried out on the solid sample. The fs-setup to carry out experiments on solid state has been described elsewhere.[33] Figure 5 shows the emission transients of the most concentrated sample (initial NR concentration of 10^{-3}M) upon excitation at 470 nm, and gating at different observation wavelengths (575 – 700 nm). The obtained parameters (τ_i, a_i) from a multi-exponential fit are shown in Table 4. The fits suggest that the emission decays are composed of four components: τ_1 = 350 – 460 fs, τ_2 = 9 ps, τ_3 = 220 ps and τ_4 = 1.33 ns. The two longest times are fixed in the fit, and correspond to the average values obtained from the TCSPC experiments for the same sample excited at the same wavelength. The 9-ps component decays at shorter wavelengths of observation, but disappears from 650 nm. The fs-component (τ_1), was recorded as a rise from 600 nm to the end of the observation range. The value of τ_2 is similar to the one (8.5 ps) previously reported for NR interacting within Al-ITQ-HB, and assigned to vibrational cooling (VC) in the excited state.[33] We attribute the fs-component to an ICT reaction in adsorbed NR molecules, owing to its molecular structure having electron donor and acceptor groups (Scheme 1A, Scheme 2). When NR is encapsulated within silica based materials (zeolites and doped MCM 41 derivates), the ICT process

was reported to occur in 200 - 400 fs.[31, 32, 39] The value of its time constant becomes longer (~ 1 ps) when NR is encapsulated within the Al-ITQ-HB framework.[33] The slowing down of this event has been explained in terms of a lower polarity and different interactions (such as H-bonds) present in the MOF than in the zeolites or mesoporous materials. However, in the present work, we observed that the ICT process when NR is adsorbed on the MOF surface is slightly faster than when it is encapsulated within its structure (~1 ps, Figure S18). The possible presence of defects, typically present on the surface of solid structures[40] can provide specific interactions which condition the dye photodynamics and facilitate the ICT and ET processes. This reflects different interactions of this molecular probe with the Al-ITQ-HB surface, and suggests possible different outcome of the catalytic reactions using this MOF when the reactants are within or on the external surface. Again, this finding using fs-resolution will help to elucidate the behavior of a well-known molecular probe interacting with a newly reported MOF, providing ideas of different ways to explore other surface and interface challenges.

4. CONCLUSIONS

In this work, we have presented and discussed, armed with fast and ultrafast spectroscopies the photobehavior of an organic dye when it is adsorbed on the surface of a novel MOF-type hybrid material, Al-ITQ-HB. The steady-state behaviour of three NR@Al-ITQ-HB hybrid complexes with $[NR]_0$ predominantly adsorbed on the surface of the MOF reveals broad absorption and narrow emission bands. The absorption and emission spectral overlap and the shape of the bands suggest possible homo energy transfer between adsorbed NR molecules. Picosecond experiments show that the time of this energy-transfer process depends on the $[NR]_0$, which is abnormally long (ns regime) and becoming shorter as the concentration increases from $1x10^{-5}$M to $1x10^{-3}$M. We compare the results with those using pellets of NR powder, as well as NR adsorbed on

the surface of SiO_2 and Al_2O_3 nanoparticles. Surprisingly, in these samples, and under ps-time resolution, we observed no evidence of an energy-transfer process. Thus, we conclude that the Al-ITQ-HB provides a unique surface environment (most probably due to the presence of surface defects and vacancies) that allows the occurrence of energy transfer between adsorbed NR molecules.

Femtosecond experiments on the NR@Al-ITQ-HB solid sample provide ~400-fs and 9-ps components assigned to an ICT reaction and vibrational cooling process, respectively. The fs-component is shorter than that recorded using NR@Al-ITQ-HB composites synthesized under different conditions. We believe that these findings provide information for a better understanding of photocatalytic reactions using this type of MOF, and can be also relevant for other hybrid systems of interest in photonics. Further experiments targeting the photobehavior of single or few molecules on the surface and within the MOF could shine more light on a topic, which is of great interest: the understanding of site specific catalytic reactions of organic molecules at short space and time scales.

ASSOCIATED CONTENT

Supporting Information

Figure S1: XRD patterns of Al-ITQ-HB and NR@Al-ITQ-HB. Figure S2: TEM images of Al-ITQ-HB. Figure S3: UV-visible absorption spectra of NR@Al-ITQ-HB composites in solid state with different $[NR]_0$. Figure S4: Emission spectra of NR@Al-ITQ-HB composites. Figures S5: Spectral overlap of NR@Al-ITQ-HB composites. Figure S6: Excitation spectra of NR@Al-ITQ-HB composites. Figure S7: Analysis of the NR@Al-ITQ-HB emission decay with different time components. Figure S8. Emission decays of NR@Al-ITQ-HB composites for different excitation wavelengths. Figure S9.

NR@Al-ITQ-HB TRES for different excitation wavelengths. Table S1. Values of the absolute spectral overlap and the time constant of the energy transfer process for each NR@Al-ITQ-HB complex. Figure S10. Spectra of NR@Al-ITQ-HB composites collected at 5 ns of delay time. Figure S11. UV-visible absorption and emission spectra of NR in solid state. Table S2: Lifetimes, pre-exponential factors and contributions obtained from the decays analysis of NR in solid state. Figure S12: UV-visible absorption spectra of NR/SiO_2 NPs at different $[NR]_0$. Figure S113: Normalized UV-visible absorption and emission spectra of NR/SiO_2 NPs at different $[NR]_0$. Figure S14: Emission decays of NR/SiO_2 NPs at different $[NR]_0$. Table S3: Lifetimes, pre-exponential factors and contributions obtained from the decays analysis of NR//SiO_2 NPs at different $[NR]_0$. Figure S15: UV-visible absorption spectra of NR/Al_2O_3 NPs at different $[NR]_0$. Figure S16: Normalized UV-visible absorption and emission spectra of NR/Al_2O_3 NPs at different initial dye concentrations $[NR]_0$. Figure S17: Emission decays of NR/Al_2O_3 NPs at different $[NR]_0$. Table S4: Lifetimes, pre-exponential factors and contributions obtained from the decays analysis of NR/Al_2O_3 at different $[NR]_0$. Figure S18: Comparison of the emission transients of Al-ITQ-HB with NR adsorbed on its surface and encapsulated within its structure.

AUTHOR INFORMATION

Corresponding Author:

*Email: Boyko.Koen@uclm.es Abderrazzak.Douhal@uclm.es

Author Contributions

Al-ITQ-HB and NR@Al-ITQ-HB composites were made by the ITQ group. The spectroscopic experiments were executed and analyzed by the UCLM group. The

manuscript was written through contributions of all authors. All authors have given approval to the final version of the manuscript.

Notes

The authors declare no competing financial interest.

ACKNOWLEDGEMENTS

This work was supported by MINECO and JCCM through projects MAT2017-82288-C2-1-P, MAT2014-57646-P and PEII-2014-003-P. J.M.M. thanks the predoctoral fellowship from the Severo Ochoa program for support (SEV-2016-0683) and E.C.M thanks the MINECO for the FPI fellowship.

REFERENCES

1. Kaskel, S., Porous Metal-Organic Frameworks. In *Handbook of Porous Solids*, Wiley-VCH Verlag GmbH: 2008; pp 1190-1249.
2. Kitagawa, S.; Kitaura, R.; Noro, S.-i., Functional Porous Coordination Polymers. *Angew. Chem. Int. Ed.* **2004,** *43*, 2334-2375.
3. Rowsell, J. L. C.; Yaghi, O. M., Metal–organic frameworks: a new class of porous materials. *Microporous Mesoporous Mater.* **2004,** *73*, 3-14.
4. Czaja, A. U.; Trukhan, N.; Muller, U., Industrial applications of metal-organic frameworks. *Chem. Soc. Rev.* **2009,** *38*, 1284-1293.
5. Getman, R. B.; Bae, Y. S.; Wilmer, C. E.; Snurr, R. Q., Review and analysis of molecular simulations of methane, hydrogen, and acetylene storage in metal-organic frameworks. *Chem. Rev.* **2012,** *112*, 703-723.
6. Li, B.; Wen, H. M.; Wang, H.; Wu, H.; Tyagi, M.; Yildirim, T.; Zhou, W.; Chen, B., A porous metal-organic framework with dynamic pyrimidine groups exhibiting record high methane storage working capacity. *J. Am. Chem. Soc.* **2014,** *136*, 6207-6210.
7. Li, J.-R.; Kuppler, R. J.; Zhou, H.-C., Selective gas adsorption and separation in metal-organic frameworks. *Chem. Soc. Rev.* **2009,** *38*, 1477-1504.
8. Murray, L. J.; Dinca, M.; Long, J. R., Hydrogen storage in metal-organic frameworks. *Chem. Soc. Rev.* **2009,** *38*, 1294-1314.
9. Ma, L.; Abney, C.; Lin, W., Enantioselective catalysis with homochiral metal-organic frameworks. *Chem. Soc. Rev.* **2009,** *38*, 1248-1256.
10. Liu, J.; Chen, L.; Cui, H.; Zhang, J.; Zhang, L.; Su, C.-Y., Applications of metal-organic frameworks in heterogeneous supramolecular catalysis. *Chem. Soc. Rev.* **2014,** *43*, 6011-6061.
11. Li, J.-R.; Sculley, J.; Zhou, H.-C., Metal–Organic Frameworks for Separations. *Chem. Rev.* **2012,** *112*, 869-932.

12. Horcajada, P.; Gref, R.; Baati, T.; Allan, P. K.; Maurin, G.; Couvreur, P.; Férey, G.; Morris, R. E.; Serre, C., Metal–Organic Frameworks in Biomedicine. *Chem. Rev.* **2012,** *112*, 1232-1268.
13. Kurmoo, M., Magnetic metal-organic frameworks. *Chem. Soc. Rev.* **2009,** *38*, 1353-1379.
14. Foster, M. E.; Azoulay, J. D.; Wong, B. M.; Allendorf, M. D., Novel metal-organic framework linkers for light harvesting applications. *Chem. Sci.* **2014,** *5*, 2081-2090.
15. So, M. C.; Wiederrecht, G. P.; Mondloch, J. E.; Hupp, J. T.; Farha, O. K., Metal-organic framework materials for light-harvesting and energy transfer. *Chem. Commun.* **2015,** *51*, 3501-3510.
16. Alarcos, N.; Cohen, B.; Ziółek, M.; Douhal, A., Photochemistry and Photophysics in Silica-Based Materials: Ultrafast and Single Molecule Spectroscopy Observation. *Chem. Rev.* **2017,** *117*, 13639-13720.
17. Yamanaka, K.-i.; Okada, T.; Goto, Y.; Ikai, M.; Tani, T.; Inagaki, S., Dynamics of Excitation Energy Transfer from Biphenylylene Excimers in Pore Walls of Periodic Mesoporous Organosilica to Coumarin 1 in the Mesochannels. *J. Phys. Chem. C* **2013,** *117*, 14865-14871.
18. Hofkens, J.; Cotlet, M.; Vosch, T.; Tinnefeld, P.; Weston, K. D.; Ego, C.; Grimsdale, A.; Mullen, K.; Beljonne, D.; Bredas, J. L.; Jordens, S.; Schweitzer, G.; Sauer, M.; De Schryver, F.; Revealing competitive Forster-type resonance energy-transfer pathways in single bichromophoric molecules. *Proc. Natl. Acad. Sci. U.S.A.* **2003,** *100*, 13146-13151.
19. Haugland, R. P.; Yguerabide, J.; Stryer, L., Dependence of the Kinectics of Singlet-Singlet Energy Transfer on Spectral Overlap. *Proc. Natl. Acad. Sci. U.S.A.* **1969,** *63*, 23-30.
20. García-García, P.; Moreno, J. M.; Díaz, U.; Bruix, M.; Corma, A., Organic–inorganic supramolecular solid catalyst boosts organic reactions in water. *Nat. Commun.* **2016,** *7*, 10835.
21. Cser, A.; Nagy, K.; Biczók, L., Fluorescence lifetime of Nile Red as a probe for the hydrogen bonding strength with its microenvironment. *Chem. Phys. Lett.* **2002,** *360*, 473-478.
22. Datta, A.; Mandal, D.; Pal, S. K.; Bhattacharyya, K., Intramolecular Charge Transfer Processes in Confined Systems. Nile Red in Reverse Micelles. *J. Phys. Chem. B* **1997,** *101*, 10221-10225.
23. Guido, C. A.; Mennucci, B.; Jacquemin, D.; Adamo, C., Planar vs. twisted intramolecular charge transfer mechanism in Nile Red: new hints from theory. *Phys. Chem. Chem. Phys.* **2010,** *12*, 8016-8023.
24. Dutta, A. K.; Kamada, K.; Ohta, K., Spectroscopic studies of nile red in organic solvents and polymers. *J. Photochem. Photobiol., A* **1996,** *93*, 57-64.
25. Ya. Freidzon, A.; Safonov, A. A.; Bagaturyants, A. A.; Alfimov, M. V., Solvatofluorochromism and twisted intramolecular charge-transfer state of the nile red dye. *Int. J. Quantum Chem* **2012,** *112*, 3059-3067.
26. Sarkar, N.; Das, K.; Nath, D. N.; Bhattacharyya, K., Twisted charge transfer processes of nile red in homogeneous solutions and in faujasite zeolite. *Langmuir* **1994,** *10*, 326-329.
27. Hazra, P.; Chakrabarty, D.; Chakraborty, A.; Sarkar, N., Intramolecular charge transfer and solvation dynamics of Nile Red in the nanocavity of cyclodextrins. *Chem. Phys. Lett.* **2004,** *388*, 150-157.

28. Maiti, N. C.; Krishna, M. M. G.; Britto, P. J.; Periasamy, N., Fluorescence Dynamics of Dye Probes in Micelles. *J. Phys. Chem. B* **1997,** *101*, 11051-11060.
29. Martin, C.; Bhattacharyya, S.; Patra, A.; Douhal, A., Single and multistep energy transfer processes within doped polymer nanoparticles. *Photochem. Photobio. Sci.* **2014,** *13*, 1241-1252.
30. Martin, C.; di Nunzio, M. R.; Cohen, B.; Douhal, A., Location and freedom of single and double guest in dye-doped polymer nanoparticles. *Photochem. Photobio. Sci.* **2014,** *13*, 1580-1589.
31. Martín, C.; Piatkowski, P.; Cohen, B.; Gil, M.; Navarro, M. T.; Corma, A.; Douhal, A., Ultrafast Dynamics of Nile Red Interacting with Metal Doped Mesoporous Materials. *J. Phys. Chem. C* **2015,** *119*, 13283-13296.
32. Martin, C.; Cohen, B.; Navarro, M. T.; Corma, A.; Douhal, A., Unraveling the ultrafast behavior of nile red interacting with aluminum and titanium co-doped MCM41 materials. *Phys. Chem. Chem. Phys.* **2016,** *18*, 2152-2163.
33. Caballero-Mancebo, E.; Cohen, B.; Moreno, J. M.; Corma, A.; Díaz, U.; Douhal, A., Exploring the Photodynamics of a New 2D-MOF Composite: Nile Red@Al–ITQ-HB. *ACS Omega* **2018,** *3*, 1600-1608.
34. Organero, J. A.; Tormo, L.; Douhal, A., Caging ultrafast proton transfer and twisting motion of 1-hydroxy-2-acetonaphthone. *Chem. Phys. Lett.* **2002,** *363*, 409-414.
35. Chen, R. F.; Knutson, J. R., Mechanism of fluorescence concentration quenching of carboxyfluorescein in liposomes: energy transfer to nonfluorescent dimers. *Analytical Biochemistry* **1988,** *172*, 61-77.
36. Meng, Q. Y.; Chen Bj Fau - Xu, W.; Xu W Fau - Zhao, X.-X.; Zhao Xx Fau - Yang, Y.-M.; Yang Ym Fau - Di, W.-H.; Di Wh Fau - Wang, X.-J.; Wang, X. J., Study on concentration quenching and energy transfer in Ln^{3+} (Ln = Tb, Tm, Eu) in Y_2O_3 nanocrystal powders. *Spectrosc. Spectral Analysis* **2009,** *29*, 151-155.
37. Kawamura, Y.; Brooks J.; Brown, J. J.; Sasabe, H.; Adachi, C. Intermolecular interaction and a concentration-quenching mechanism of phosphorescent Ir(III) complexes in a solid film. *Phys. Rev. Lett.* **2006,** *96*, 017404-1 - 017404-4.
38. Gil, M.; Ziółek, M.; Organero, J. A.; Douhal, A., Confined Fast and Ultrafast Dynamics of a Photochromic Proton-Transfer Dye within a Zeolite Nanocage. *J. Phys. Chem. C* **2010,** *114*, 9554-9562.
39. di Nunzio, M. R.; Caballero-Mancebo, E.; Martín, C.; Cohen, B.; Navarro, M. T.; Corma, A.; Douhal, A., Femto-to nanosecond photodynamics of Nile Red in metal-ion exchanged faujasites. *Microporous Mesoporous Mater.* **2018,** *256*, 214-226.
40. Halbherr, O.; Fischer, R. A., Defects and Disorder in MOFs. In *The Chemistry of Metal–Organic Frameworks*, Wiley-VCH Verlag GmbH & Co. KGaA: 2016; pp 795-822.

FIGURES, TABLES AND SCHEMES

Captions

Table 1. Values of the fluorescence emission lifetimes (τ_i) and normalized (to 100) pre-exponential factors (a_i) obtained from a global multi-exponential fit of the emission decays of NR@Al-ITQ-HB with $1x10^{-5}$M of initial dye concentration ($[NR]_0$) upon excitation at different wavelengths.

Table 2. Values of the parameters used in the global multi-exponential fit of the emission decays of NR@Al-ITQ-HB with initial NR concentration of $1x10^{-4}$M upon excitation at different wavelengths.

Table 3. Values of the fluorescence emission lifetimes (τ_i) and normalized (to 100) pre-exponential factors (a_i) obtained from a global multi-exponential fit of the emission decays of NR@Al-ITQ-HB with initial NR concentration $1x10^{-3}$M upon excitation at different wavelengths.

Table 4. Values of the time constants and normalized (to 100) pre-exponential factors (a_i) obtained from a multiexponential fit of the femtosecond emission transients of NR@Al-ITQ-HB with $1x10^{-3}$M of $[NR]_0$ upon excitation at 470 nm and observation as indicated. The negative sign for a_i indicates a rising component in the emission signal.

Figure 1. UV-visible absorption and emission spectra of NR@Al-ITQ-HB composites using different $[NR]_0$: $1x10^{-5}$M (blue solid line), $1x10^{-4}$M (green dots) and $1x10^{-3}$M (yellow points/lines). The emission spectra were recorded upon excitation at 470 nm.

Figure 2. Normalized magic-angle emission decays of NR@Al-ITQ-HB with linear and logarithmic plots at different initial NR concentrations: $1x10^{-5}$M (A and A'), $1x10^{-4}$M (B and B') and $1x10^{-3}$M (C and C') upon excitation at 470 nm, and observation at different

wavelengths. The solid lines are from the best global fits using a multiexponential function. The dashed line shows the instrument response function (IRF ~70 ps).

Figure 3. Normalized Time-Resolved Emission Spectra (TRES) of NR@Al-ITQ-HB with $1x10^{-5}$M (A, A', A''), $1x10^{-4}$M (B, B', B'') and $1x10^{-3}$M (C, C', C'') of $[NR]_0$. The excitation wavelengths were 470 (A, B, C), 550 (A', B', C') and 635 nm (A'', B'', C''). The insert shows the gating times upon ps-excitation.

Figure 4. (A) Emission decays of NR in solid state upon excitation at 470 nm and observation at different wavelengths. (B, C and D) Comparison of representative emission decays of (1) NR@Al-ITQ-HB, (2) NR/Al_2O_3 NPs and (3) NR/SiO2 NPs at three different $[NR]_0$, respectively. The excitation and emission wavelengths were 470 and 750 nm, respectively.

Figure 5. Femtosecond emission transients of NR@Al-ITQ-HB in solid state with $1x10^{-3}$M of initial NR concentration upon excitation at 470 nm and observation at different wavelengths. The solid lines are from the best fits using a multiexponential function. The dashed line is the IRF (~300 fs) of the set up.

Scheme 1. (A) Cartoon (not in scale) illustrating the adsorption of Nile Red (NR) on the Al-ITQ-HB surface. The zoom shows the topology and structure of the MOF and possible location of adsorbed NR molecules. (B) Pictures of the different studied composites. NR@Al-ITQ-HB (I) sample was prepared and washed several times until no NR was observed in the supernatant, while NR@Al-ITQ-HB (II) was prepared and solvent evaporated as described in this work.

Scheme 2. Photophysical scheme (not in scale) giving information on the spectral and dynamical behaviour of NR@Al-ITQ-HB composites. LE, ICT and CS mean local

excited state, intramolecular charge transfer and charge separated state, respectively. See text for more details.

Table 1.

	λ_{exc} = 470 nm						**λ_{exc} = 550 nm**						**λ_{exc} = 635 nm**					
λ_{obs}/nm	**τ_1/ns** (±0.05)	**a_1**	**τ_2/ns** (±0.20)	**a_2**	**τ_3/ns** (±0.20)	**a_3**	**τ_1/ns** (±0.05)	**a_1**	**τ_2/ns** (±0.20)	**a_2**	**τ_3/ns** (±0.20)	**a_3**	**τ_1/ns**	**a_1**	**τ_2/ns** (±0.20)	**a_2**	**τ_3/ns** (±0.20)	**a_3**
550		30		62		8												
575		22		58		25												
600		19		56		41		12		54		34						
625		6		53		83		4		20		76						
650	**0.46**	-	**2.50**	17	**4.77**	100	**0.38**	-	**2.06**	-100	**4.53**	100	-	-	**2.71**	61	**4.68**	39
675		-		-100		100		-		-100		100		-		60		40
700		-		-100		100		-		-100		100		-		61		39
725		-		-100		100		-		-100		100		-		61		39
750		-		-100		100		-		-100		100		-		61		39

Table 2.

	λ_{exc} = 470 nm						**λ_{exc} = 550 nm**						**λ_{exc} = 635 nm**					
λ_{obs}/nm	**τ_1/ns** (±0.05)	**a_1**	**τ_2/ns** (±0.20)	**a_2**	**τ_3/ns** (±0.20)	**a_3**	**τ_1/ns** (±0.05)	**a_1**	**τ_2/ns** (±0.20)	**a_2**	**τ_3/ns** (±0.20)	**a_3**	**τ_1/ns**	**a_1**	**τ_2/ns**	**a_2**	**τ_3/ns** (±0.20)	**a_3**
550		38		53		9												
575		36		54		10												
600		22		53		25		21		58		21						
625		3		17		80		5		34		61						
650	**0.32**	-10	**2.75**	-90	**4.90**	100	**0.33**	-	**2.21**	-100	**4.96**	100	-	-	-	-	**4.67**	100
675		-8		-92		100		-		-100		100		-		-		100
700		-5		-95		100		-		-100		100		-		-		100
725		-5		-95		100		-		-100		100		-		-		100
750		-5		-95		100		-		-100		100		-		-		100

Table 3.

	λ_{exc} = 470 nm						λ_{exc} = 550 nm						λ_{exc} = 635 nm					
λ_{obs}/nm	τ_1/ns (±0.05)	a_1	τ_2/ns (±0.20)	a_2	τ_3/ns (±0.20)	a_3	τ_1/ns (±0.05)	a_1	τ_2/ns (±0.20)	a_2	τ_2/ns (±0.20)	a_2	τ_1/ns (±0.05)	a_1	τ_2/ns (±0.20)	a_2	τ_3/ns (±0.20)	a_3
550		88		8		4												
575		74		19		6												
600		32		42		26		75		20		5						
625		2		26		72		37		42		21						
650	**0.22**	-100	**1.33**	27	**3.61**	73	**0.16**	-100	**1.30**	28	**2.76**	72	**0.15**	25	**1.39**	35	**3.10**	40
675		-100		12		88		-100		4		96		9		24		67
700		-100		11		89		-100		5		95		16		21		63
725		-100		6		94		-100		-		100		11		20		69
750		-100		-		100		-100		-		100		8		14		78

Table 4.

λ_{Obs}/nm	τ_1/fs (±50)	a_1	τ_2/ps (±0.5)	a_2	τ_3/ps	a_3	τ_4/ns	a_4
575	-	-	9.0	20		80	-	-
600	350	-100	9.1	15		85	-	-
625	400	-100	9.0	4	220*	82		14
650	450	-69	-	-		-31	1.4*	100
675	460	-60	-	-		-40		100
700	460	-40	-	-		-60		100

*Fixed values in the fit.

Figure 1.

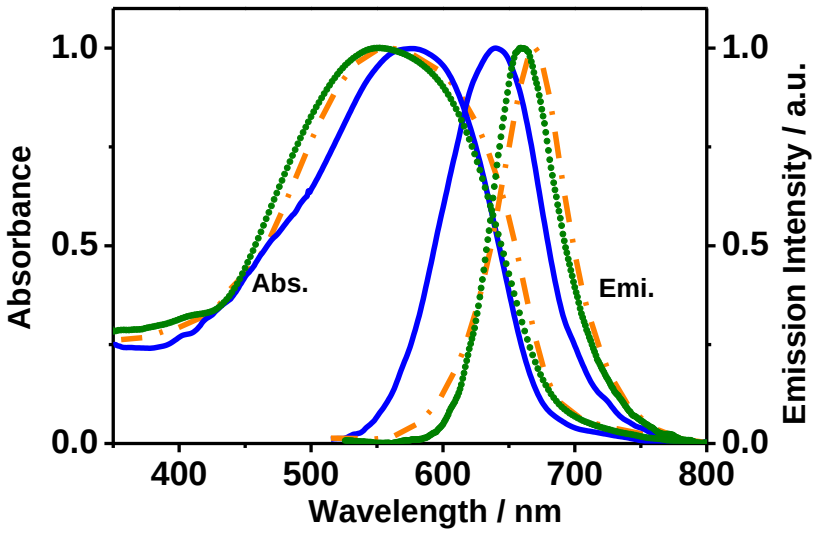

Figure 2.

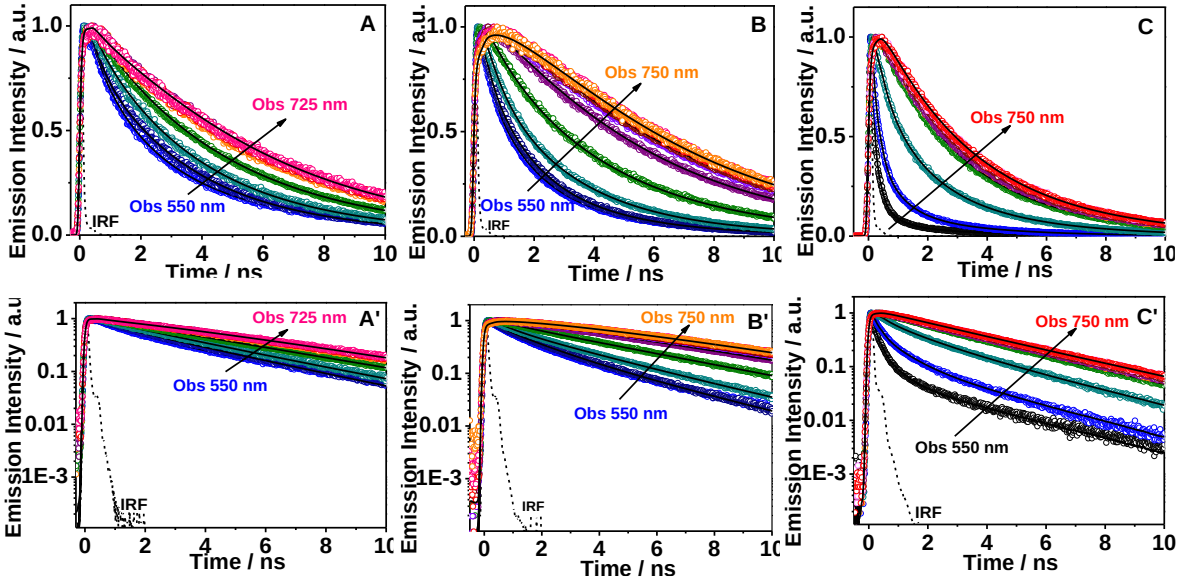

Figure 3.

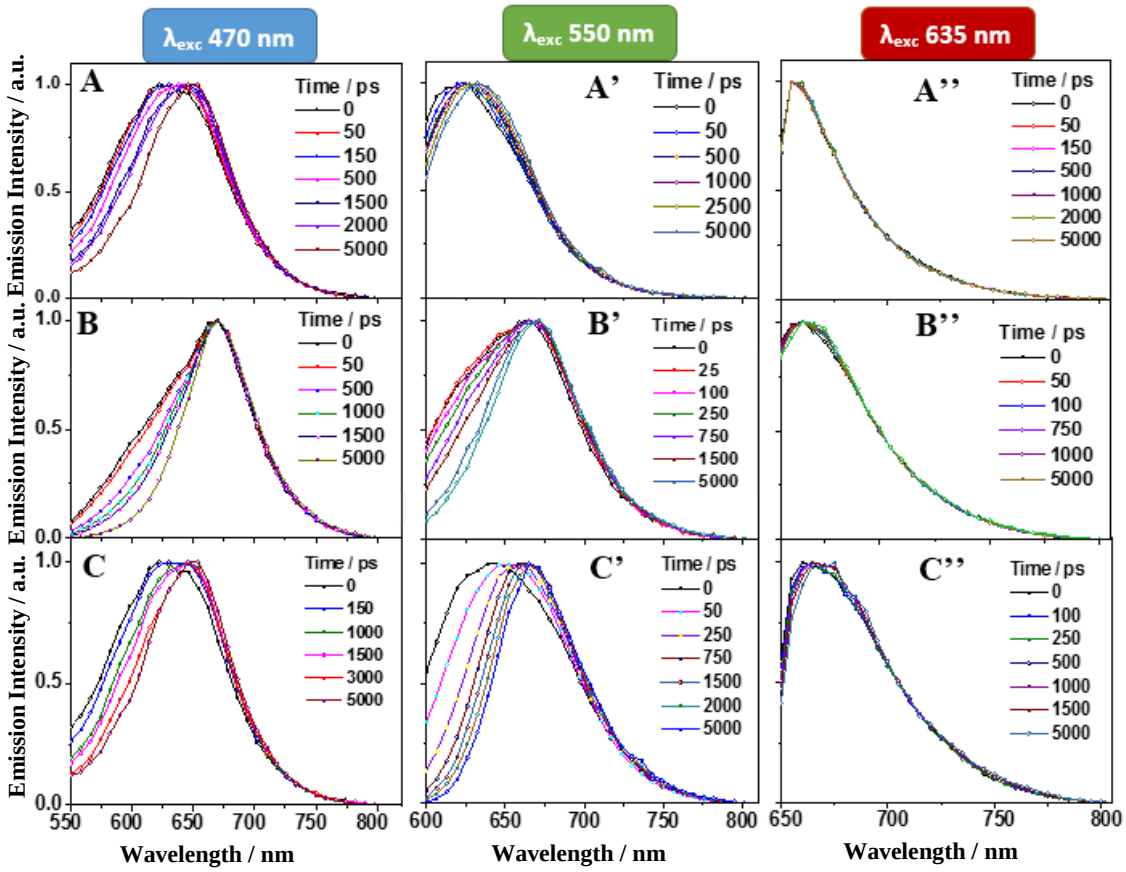
λexc 470 nm
λexc 550 nm
λexc 635 nm
A
A'
A''
B
B'
B''
C
C'
C''
Time / ps
Emission Intensity / a.u.
Wavelength / nm

Figure 4.

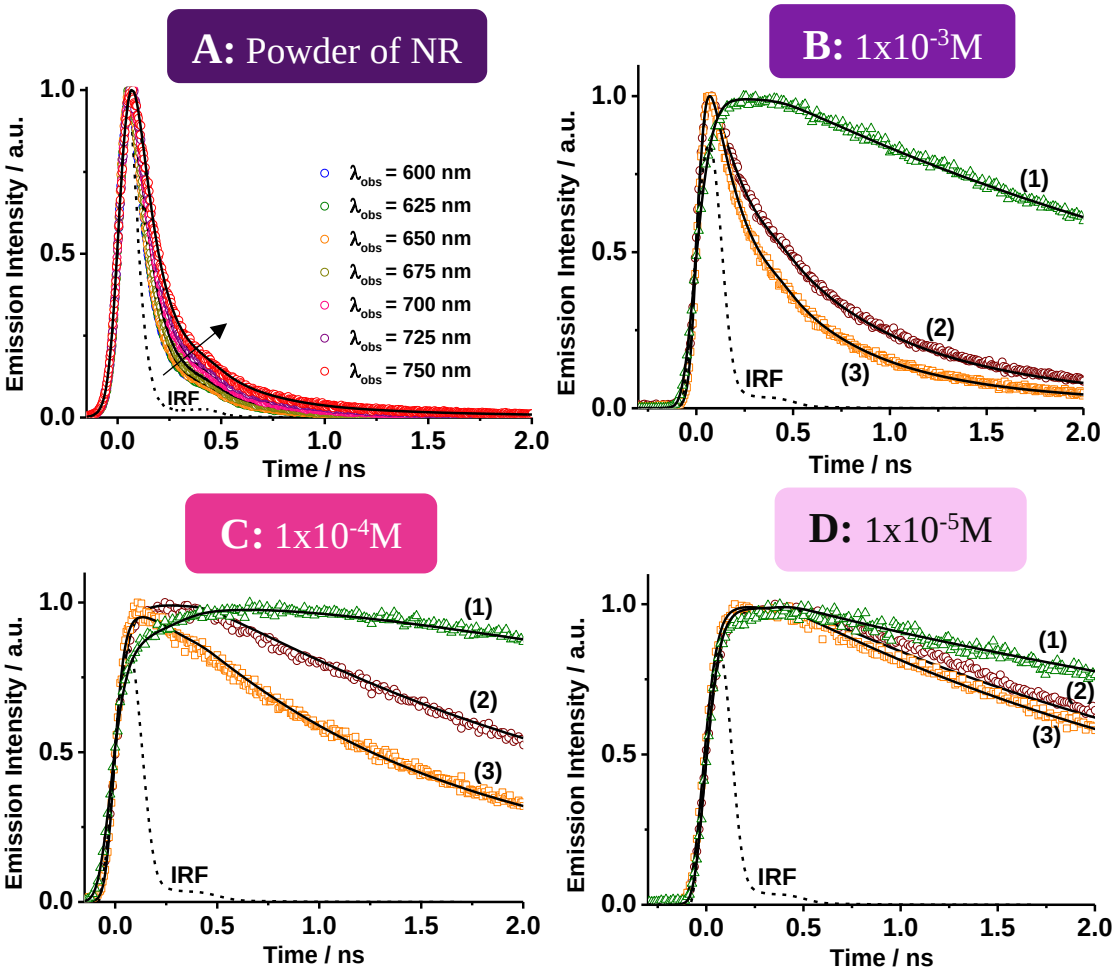

Figure 5.

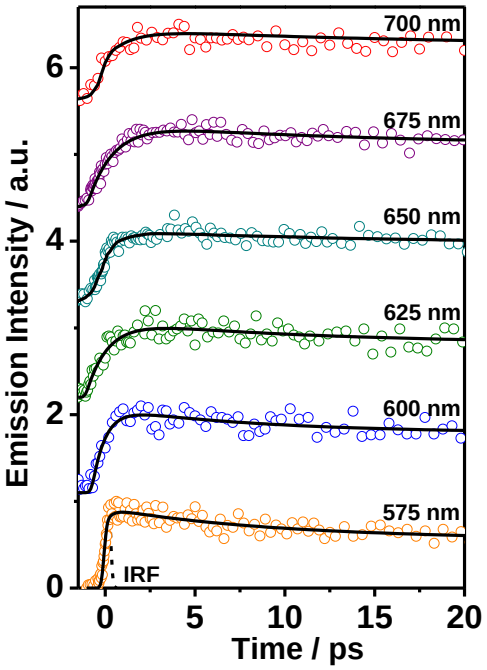

Scheme 1.

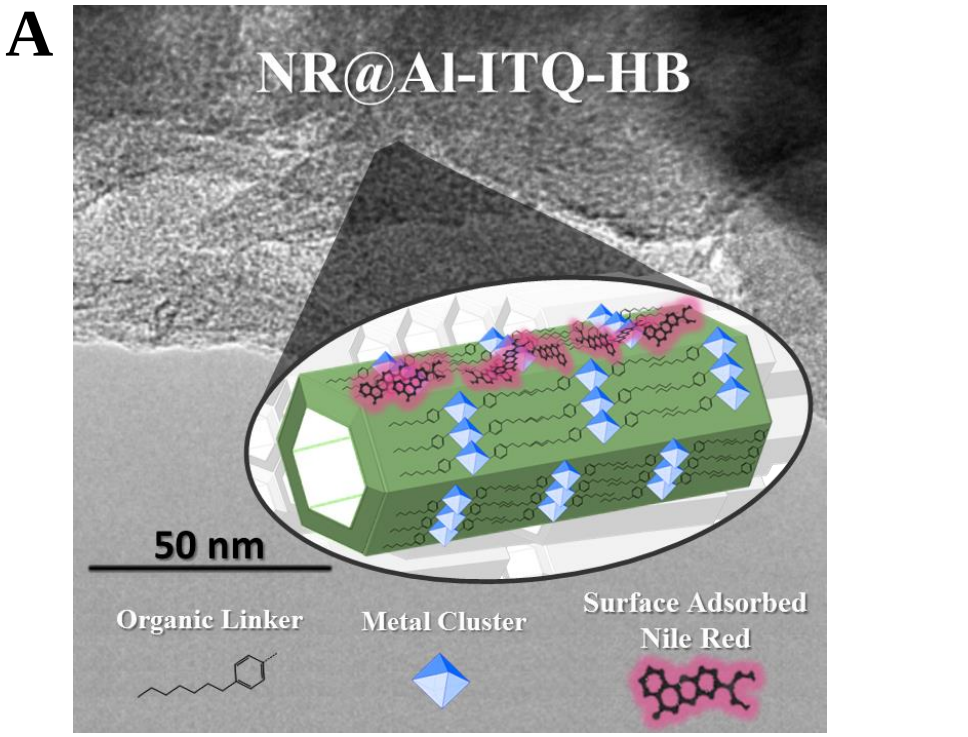
A
NR@Al-ITQ-HB
50 nm
Organic Linker
Metal Cluster
Surface Adsorbed
Nile Red

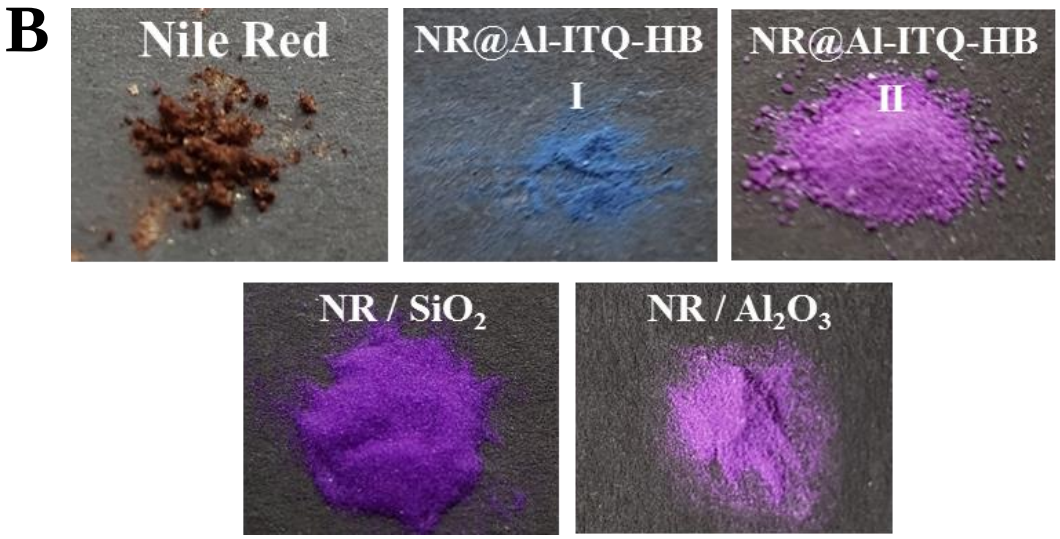
B
Nile Red
NR@Al-ITQ-HB
I
NR@Al-ITQ-HB
II
NR / SiO2
NR / Al2O3

Scheme 2.

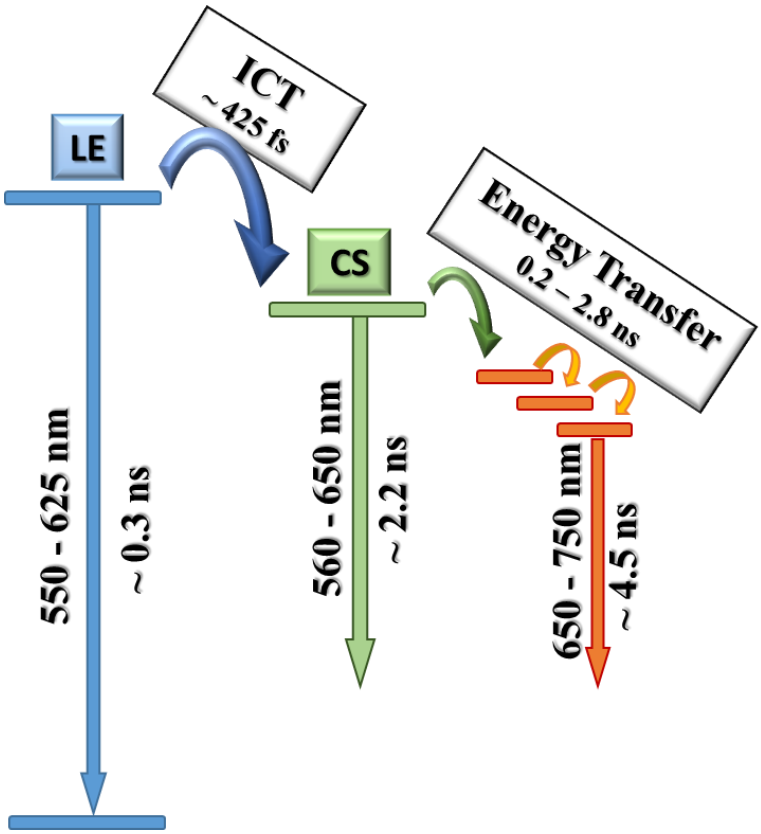
LE
ICT
~ 425 fs
CS
Energy Transfer
0.2 – 2.8 ns
550 - 625 nm
~ 0.3 ns
560 - 650 nm
~ 2.2 ns
650 - 750 nm
~ 4.5 ns

Table of Contents: